

Nature of hyperfine interactions in TbPc_2 single-molecule magnets: Multireference *ab-initio* study

Aleksander L. Wysocki* and Kyungwha Park*

Department of Physics, Virginia Tech, Blacksburg, Virginia 24061, United States

E-mail: alexwysocki2@gmail.com; kyungwha@vt.edu

Abstract

Lanthanide-based single-ion magnetic molecules can have large magnetic hyperfine interactions as well as large magnetic anisotropy. Recent experimental studies reported tunability of these properties by changes of chemical environments or by application of external stimuli for device applications. In order to provide insight onto the origin and mechanism of such tunability, here we investigate the magnetic hyperfine and nuclear quadrupole interactions for ^{159}Tb nucleus in TbPc_2 (Pc=phthalocyanine) single-molecule magnets using multireference *ab-initio* methods including spin-orbit interaction. Since the electronic ground and first-excited (quasi)doublets are well separated in energy, the microscopic Hamiltonian can be mapped onto an effective Hamiltonian with an electronic pseudo-spin $S = 1/2$. From the *ab-initio*-calculated parameters, we find that the magnetic hyperfine coupling is dominated by the interaction of the Tb nuclear spin with electronic orbital angular momentum. The asymmetric $4f$ -like electronic charge distribution leads to a strong nuclear quadrupole interaction with significant non-axial terms for the molecule with low symmetry. The *ab-initio* calculated

electronic-nuclear spectrum including the magnetic hyperfine and quadrupole interactions is in excellent agreement with experiment. We further find that the non-axial quadrupole interactions significantly influence the avoided level crossings in magnetization dynamics and that the molecular distortions affect mostly the Fermi contact terms as well as the non-axial quadrupole interactions.

Introduction

Lanthanide-based single-ion magnetic molecules¹⁻⁹ have drawn a lot of attention due to superior magnetic properties, structural compatibility with substrates, and proof-of-concept experiments for magnetic information storage and quantum information science applications. Recently, molecular crystals of dysprosium-based single-ion magnetic molecules have shown magnetic hysteresis above liquid nitrogen temperature⁶ and an experimental effective energy barrier over 1000 cm^{-1} .⁷ Especially, double-decker $[\text{LnPc}_2]$ (Pc=phthalocyanine) single-molecule magnets (SMMs)¹⁰ are shown to form periodic layers on substrates.¹¹⁻¹³ Furthermore, the terbium (Tb) nuclear magnetic moment was found to be strongly coupled to the electronic degrees of freedom in TbPc_2 SMMs.¹⁴⁻¹⁷ By taking advantage of a strong hyperfine Stark effect, the Tb nuclear levels in a TbPc_2 SMM have been used for experimental realizations of Rabi oscillations,⁸ Ramsey interferometry,¹⁸ and Grover's algorithm⁹ within a single-molecule transistor platform.

In TbPc_2 SMMs, one Tb^{3+} ion is sandwiched between two approximately planar Pc ligands (Fig. 1). Three different oxidation states (-1 , 0 , and $+1$) were experimentally realized.¹⁹⁻²⁵ The synthesized TbPc_2 molecules have only approximate D_{4d} symmetry. The degree of symmetry deviation varies with crystal packing, diamagnetic dilution molecules, or solvent molecules used in synthesis processes.

The $4f^8$ electronic configuration of the Tb^{3+} ion results in electron spin and orbital angular momentum of $S = 3$ and $L = 3$, respectively. When the strong spin-orbit interaction (SOI) is combined with the ligand crystal field (CF), the Tb ion with the total angular

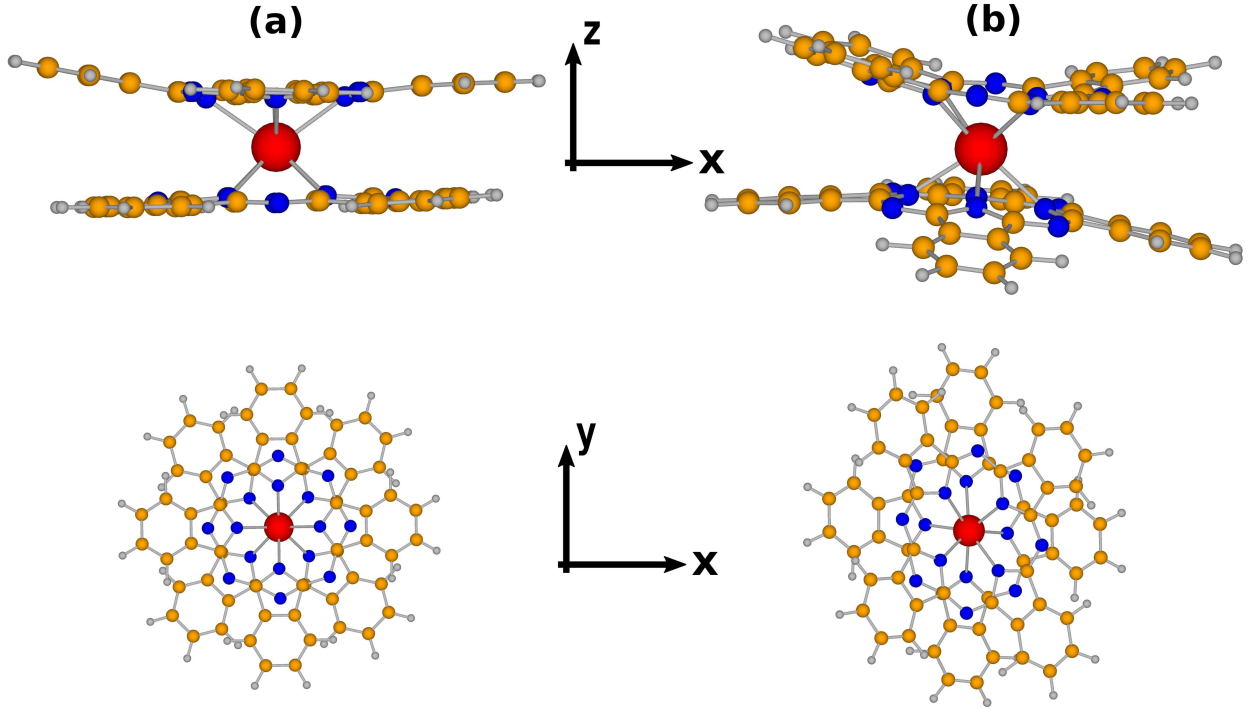


Figure 1: Side and top views of experimental structure of two TbPc_2 molecules of interest. (a) Neutral TbPc_2 with geometry from Ref. 19. (b) Anionic TbPc_2 with geometry from Ref. 20. Red, blue, orange, and gray spheres represent Tb, N, C, and H atoms, respectively. The coordinate system corresponds to magnetic axes obtained by diagonalization of the \mathbf{g} matrix calculated for the ground (quasi)doublet for each molecule.

momentum $J = 6$ acquires large magnetic anisotropy and magnetic easy axis approximately perpendicular to the Pc planes. For cationic or anionic TbPc_2 SMMs, the ground $J = 6$ multiplet is very well separated from excited multiplets. The lowest quasi-doublet ($M_J = \pm 6$) in the ground J -multiplet is separated from the first-excited quasi-doublet by $\sim 300 \text{ cm}^{-1}$ (Fig. 2),^{26,27} where M_J is the total angular momentum projected onto the magnetic easy axis. For neutral TbPc_2 SMMs, one unpaired electron (with spin $s = 1/2$) is delocalized within the two Pc ligands. This ligand spin interacts with the Tb multiplets and doubles the number of low-energy levels. In addition, this extra electron makes neutral TbPc_2 a Kramers system. The ground doublet can be represented by $M_J = \pm 6$ coupled to the ligand spin parallel to the Tb angular momentum. The first-excited doublet lies $\sim 8 \text{ cm}^{-1}$ above and it can be represented by $M_J = \pm 6$ coupled to the ligand spin anti-parallel to the Tb angular momentum (Fig. 2).²⁶

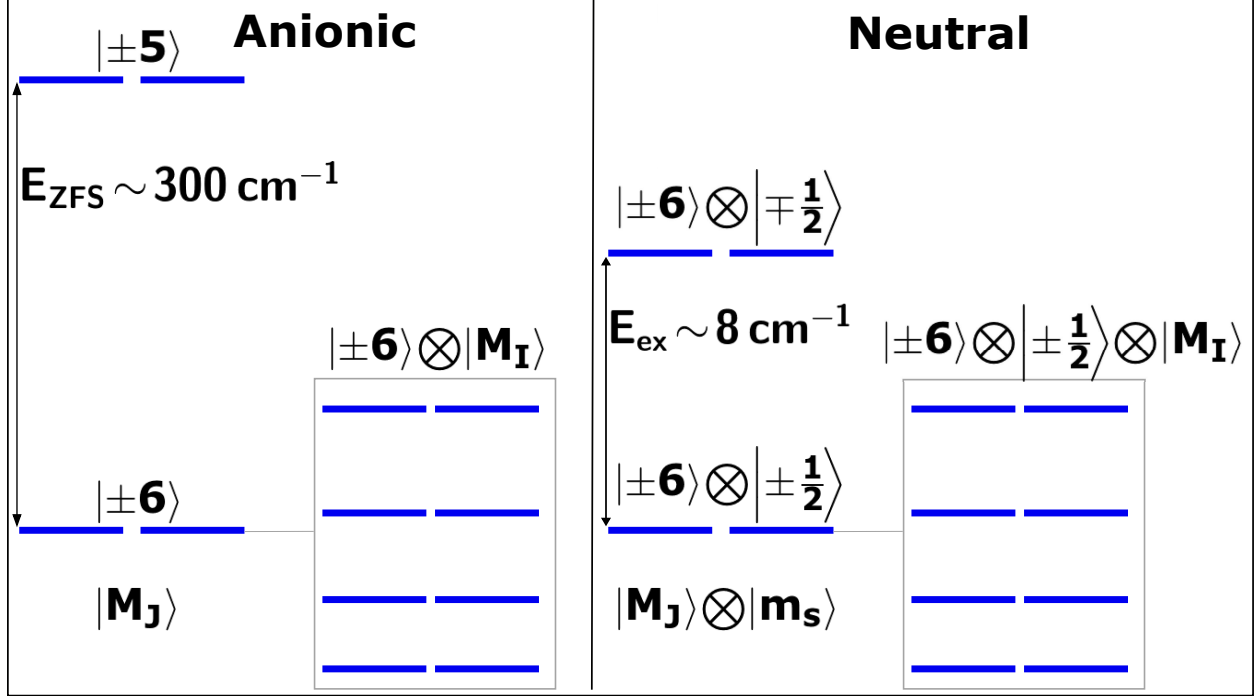


Figure 2: Schematic illustration of the low-energy electronic-nuclear spectrum for the anionic and neutral TbPc_2 molecules. For the anionic molecule, the electronic ground quasi-doublet $|M_J = \pm 6\rangle$ is well isolated from the first excited quasi-doublet ($E_{\text{ZFS}} \sim 300 \text{ cm}^{-1}$). For the neutral molecule, the electronic ground doublet $|M_J = \pm 6\rangle \otimes |m_s = \pm 1/2\rangle$ is separated by a gap of $\sim 8 \text{ cm}^{-1}$ from the first-excited doublet that differs by a relative orientation of the ligand spin and Tb angular momentum. For the anionic and neutral TbPc_2 , the hyperfine interaction with the Tb nuclear spin $I = 3/2$ splits each state of the electronic ground (quasi)doublet into four states. Here $|M_I\rangle$ and $|m_s\rangle$ correspond to the nuclear spin and the ligand spin, respectively. Modified from Ref. 26.

^{159}Tb nucleus has the natural abundance of 100% and its nuclear spin is $I = 3/2$. Therefore, the Tb nuclear spin couples to the electronic spin and orbital angular momentum, which splits each electronic state into four states. Since $I > 1/2$, the nuclear quadrupole interaction must also be present in TbPc_2 SMMs. Taking the ground $J = 6$ multiplet into account, observed magnetic hysteresis loops were fitted to a simplified model with two parameters such as a magnetic hyperfine coupling constant and an axial nuclear quadrupole parameter.²⁸ However, there are no *ab-initio* studies on the nature and mechanism of the magnetic hyperfine and nuclear quadrupole interactions in these SMMs. Density-functional theory cannot be used for such studies because the Tb^{3+} ion has large orbital angular momentum

as well as almost degenerate $4f$ orbitals.

Here we investigate the magnetic hyperfine and nuclear quadrupole interactions for anionic and neutral TbPc_2 molecules using *ab-initio* multireference calculations including SOI. We evaluate the interaction parameters and analyze their physical and chemical origin. We then construct the effective pseudo-spin Hamiltonian from which the electronic-nuclear low-energy spectrum is found. Our results unambiguously show the necessity of using multireference methods including SOI for the proposed study. Next, we calculate the Zeeman diagram and discuss the role of the magnetic hyperfine and nuclear quadrupole interactions in magnetization dynamics. Finally, we investigate the effect of molecular distortions on these interactions.

Methodology

In the following we use SI units. Quantum-mechanical operators are denoted by hats. Vectors, tensors and matrices are written in a bold font.

Magnetic hyperfine interactions

Consider a non-relativistic electron with a mass m , a linear momentum $\hat{\mathbf{p}}$, and a spin $\hat{\mathbf{s}}$ in the presence of a vector potential $\hat{\mathbf{A}}_N$ induced by a nuclear spin moment $\hat{\mathbf{I}}$ where the nucleus is located at the origin. The microscopic Hamiltonian \hat{H}_{MHF} for such an electron can be written as²⁹

$$\hat{H}_{\text{MHF}} = \frac{1}{2m} \left(\hat{\mathbf{p}} + e\hat{\mathbf{A}}_N \right)^2 + g_e\mu_B(\nabla \times \hat{\mathbf{A}}_N) \cdot \hat{\mathbf{s}}, \quad (1)$$

where g_e is the electronic g -factor, μ_B is Bohr magneton, and $\hat{\mathbf{A}}_N = \hat{\mathbf{m}}_N \times \mathbf{r}/r^3$. Here $\hat{\mathbf{m}}_N = g_N\mu_N\hat{\mathbf{I}}$ denotes the nuclear magnetic moment, where g_N is the nuclear g -factor (that is 1.34267 for Tb), μ_N is the nuclear magneton, and \mathbf{r} is the position vector of the electron with respect to the nucleus. Keeping only the first-order terms in $\hat{\mathbf{A}}_N$, this Hamiltonian can

be decomposed into three contributions such as

$$\hat{H}_{\text{MHf}} = \hat{H}_{\text{PSO}} + \hat{H}_{\text{SD}} + \hat{H}_{\text{FC}}. \quad (2)$$

The first term in Eq. (2) is the paramagnetic spin-orbital (PSO) contribution that describes the interaction between the electronic orbital angular momentum $\hat{\mathbf{L}}$ and the nuclear magnetic moment

$$\hat{H}_{\text{PSO}} = \frac{\mu_0 \mu_B}{2\pi} \frac{1}{r^3} \hat{\mathbf{L}} \cdot \hat{\mathbf{m}}_N, \quad (3)$$

where μ_0 is the vacuum permeability. The second term in Eq. (2) describes the spin dipolar (SD) interaction between the nuclear magnetic moment and the electronic spin moment $\hat{\mathbf{m}}_s = g_e \mu_B \hat{\mathbf{S}}$

$$\hat{H}_{\text{SD}} = \frac{\mu_0}{4\pi} \frac{1}{r^3} \left[\hat{\mathbf{m}}_s \cdot \hat{\mathbf{m}}_N - 3 \frac{(\hat{\mathbf{m}}_s \cdot \mathbf{r})(\hat{\mathbf{m}}_N \cdot \mathbf{r})}{r^2} \right]. \quad (4)$$

Finally, \hat{H}_{FC} represents the Fermi contact (FC) interaction between the spin density at the nucleus position and the nuclear magnetic moment

$$\hat{H}_{\text{FC}} = -\frac{\mu_0}{4\pi} \frac{8\pi}{3} \hat{\mathbf{m}}_s \cdot \hat{\mathbf{m}}_N \delta(\mathbf{r}), \quad (5)$$

where $\delta(\mathbf{r})$ is a three-dimensional Dirac delta function. Note that for a Tb^{3+} ion with large orbital angular momentum, the non-relativistic form of magnetic hyperfine operator, Eqs. (2-5), is a good approximation.³⁰

For both the anionic and neutral TbPc_2 SMMs, the energy gap between the electronic ground and excited (quasi)doublets is much greater than the scale of the magnetic hyperfine interaction ($\sim 0.1 \text{ cm}^{-1}$). Therefore, for the low-energy electronic-nuclear spectrum only the ground (quasi)doublet (Fig. 2) is relevant and it can be represented by a fictitious pseudo-spin $S = 1/2$. The pseudo-spin then interacts with the magnetic field produced by the Tb nuclear spin $I = 3/2$. The effective pseudo-spin Hamiltonian for this magnetic hyperfine

interaction can be written as²⁹

$$\hat{H}_A = \hat{\mathbf{I}} \cdot \mathbf{A} \cdot \hat{\mathbf{S}}, \quad (6)$$

where \mathbf{A} is the magnetic hyperfine matrix. In order to understand degrees of mixing among $|M_S, M_I\rangle$ levels, it is convenient to rewrite the above using the ladder operators

$$\hat{H}_A = \frac{A_{zz}}{2} \hat{I}_z \hat{S}_z + \frac{A_0}{2} \hat{I}_+ \hat{S}_- + A_1 \left(\hat{I}_- \hat{S}_z + \hat{I}_z \hat{S}_- \right) + \frac{A_2}{2} \hat{I}_- \hat{S}_- + \text{h.c.}, \quad (7)$$

where h.c. denotes Hermitian conjugated terms. Here, we introduce complex parameters that are combinations of elements of the \mathbf{A} matrix

$$A_0 = \frac{1}{2} (A_{xx} + A_{yy}), \quad (8)$$

$$A_1 = \frac{1}{2} (A_{xz} + iA_{yz}), \quad (9)$$

$$A_2 = \frac{1}{2} (A_{xx} - A_{yy}) + iA_{xy}. \quad (10)$$

For pseudo-spin $S = 1/2$, the eigenvalues of the effective pseudo-spin Hamiltonian, Eq. (6), are analytically known,²⁹ and so they can be mapped onto the eigenvalues of the microscopic Hamiltonian, Eq. (2), obtained from the *ab initio* methods, in order to evaluate the \mathbf{A} matrix.^{30,31} We can determine only the magnitude of the matrix elements because the eigenvalues of Eq. (6) are expressed in terms of the elements of $(\mathbf{A}\mathbf{A}^T)$ tensor:

$$(\mathbf{A}\mathbf{A}^T)_{\alpha\beta} = 2 \sum_{ij} \langle i | \hat{h}_{\text{MHf}}^\alpha | j \rangle \langle j | \hat{h}_{\text{MHf}}^\beta | i \rangle, \quad (11)$$

where $\alpha, \beta = x, y, z$ and $\hat{h}_{\text{MHf}}^\alpha \equiv \partial \hat{H}_{\text{MHf}} / \partial \hat{I}_\alpha$. The summation runs over the *ab initio* electronic ground (quasi)doublet ($i = 1, 2$).

Nuclear quadrupole interactions

A nucleus with $I > 1/2$ has a nonzero quadrupole moment which interacts with an electric-field gradient at the nucleus position. The electric-field gradient operator $\hat{V}_{\alpha\beta}$ is given by $\frac{\partial^2\Phi}{\partial x_\alpha\partial x_\beta}$,³² where Φ is the electrostatic potential produced by the electronic charge density and other nuclei at the position of the nucleus of interest. The quadrupole interaction can be described by the following effective Hamiltonian:²⁹

$$\hat{H}_Q = \hat{\mathbf{I}} \cdot \mathbf{P} \cdot \hat{\mathbf{I}} \quad (12)$$

where \mathbf{P} is the nuclear quadrupole tensor. The components of \mathbf{P} are related to the expectation value of $\hat{V}_{\alpha\beta}$ over the *ab-initio* electronic states by the following:

$$P_{\alpha\beta} = \frac{Q}{2I(2I-1)} \langle \hat{V}_{\alpha\beta} \rangle, \quad (13)$$

where Q is the quadrupole constant that for Tb nucleus is 1432.8 mbarn.³³ In order to understand the amount of mixing among different $|M_I\rangle$ levels, we rewrite Eq. (12) using the ladder operators such as

$$\hat{H}_Q = \frac{3}{4}P_{zz} \left[\hat{I}_z^2 - \frac{I(I+1)}{3} \right] + P_1 \left(\hat{I}_z \hat{I}_- + \hat{I}_- \hat{I}_z \right) + \frac{P_2}{2} \hat{I}_-^2 + \text{h.c.}, \quad (14)$$

where complex quadrupole parameters are

$$P_1 = P_{xz} + iP_{yz}, \quad (15)$$

$$P_2 = \frac{1}{2}(P_{xx} - P_{yy}) + iP_{xy}. \quad (16)$$

Computational details

The *ab initio* calculations are performed using the MOLCAS quantum chemistry code (version 8.2).³⁴ Scalar relativistic effects are included based on the Douglas-Kroll-Hess Hamiltonian^{35,36} using relativistically contracted atomic natural orbital (ANO-RCC) basis sets.^{37,38} In particular, polarized valence triple- ζ quality (ANO-RCC-VTZP) is used for the Tb ion, and polarized valence double- ζ quality (ANO-RCC-VDZP) is used for the nitrogen and carbon atoms. Valence double- ζ quality (ANO-RCC-VDZ) is used for the hydrogen atoms. This choice of the basis set was shown to produce an accurate description of the low-energy electronic levels of TbPc₂-type molecules.²⁶

Electronic structure is calculated in two steps. In the first step, in the absence of SOI, for a given spin multiplicity, the spin-free eigenstates are obtained using state-averaged complete active space self-consistent field (SA-CASSCF) method.^{39,40} For the anionic TbPc₂, the active space consists of eight electrons and seven *4f*-like orbitals. For the neutral TbPc₂, an additional electron and a ligand orbital are included in the active space. We check that inclusion of extra ligand orbitals in the active space does not significantly affect calculated magnetic hyperfine and nuclear quadrupole interaction parameters (see Tables S1 and S2 in the Supporting Information). For the anionic TbPc₂, we consider only $S = 3$ configuration that corresponds to the Tb³⁺ spin. For the neutral TbPc₂, depending on whether ligand electron spin is parallel or antiparallel to the Tb³⁺ spin, we have two possible values of the total spin of the molecule: $S = 7/2$ or $S = 5/2$. Both spin configurations are included in the CASSCF calculations because they lie close in energy. For a given spin configuration in both the anionic and neutral molecules, we evaluate seven lowest spin-free states (roots) that roughly correspond to seven configurations of eight electrons in Tb *4f*-type orbitals. These seven spin-free states are used in the CASSCF state-averaged procedure. In the second step, SOI is included within the atomic mean-field approximation,⁴¹ in the aforementioned spin configurations and spin-free eigenstates, using the restricted active space state-interaction (RASSI) method.⁴² The resulting electronic structure agrees well with previous works.^{26,27}

Having obtained the electronic structure, we calculate the \mathbf{A} matrix according to Eq. (11) by evaluating the matrix elements of PSO, SD, and FC contributions within the ground (quasi)doublet. In MOLCAS version 8.2, only FC and SD contributions are included.³¹ Therefore, we implement the PSO term in the MOLCAS code. The main ingredient of the implementation is the evaluation of the one-electron integrals for the $\hat{\mathbf{L}}/r^3$ operator. This is done by modification of the AMFI module. We test our implementation by calculating the \mathbf{A} matrix for CN, NpF₆ and UF₆⁻ molecules (Table S3 in Supporting Information). As shown, our calculations agree well with the literature.^{31,43} The nuclear quadrupole tensor elements are calculated using Eq. (13) by evaluating the matrix elements of $\hat{V}_{\alpha\beta}$ between the ground (quasi)doublet. Note that this capability already exists in MOLCAS version 8.2.

Results and Discussion

We consider two TbPc₂ molecules: (1) neutral TbPc₂ with experimental geometry from Ref. 19 (Fig. 1a) and (2) anionic TbPc₂ with experimental geometry from Ref. 20 (Fig. 1b). The structural deviations from D_{4h} symmetry are much stronger for the anionic molecule. The ground state of the neutral molecule is a Kramers doublet which can be characterized by $M_J = \pm 6$ and the ligand spin parallel to the Tb angular momentum. On the other hand, for the anionic molecule, the ground state is $M_J = \pm 6$ quasidoublet with tunnel splitting of ~ 140 MHz. For both molecules, the electronic (quasi)doublet can be represented by a fictitious pseudo-spin $S = 1/2$.

It is convenient to present the calculated \mathbf{A} matrix and \mathbf{P} tensor in the magnetic coordinate system (Fig. 1) in which the \mathbf{g} matrix for the ground (quasi)doublet is diagonal. The \mathbf{g} matrix has only one nonzero eigenvalue for the anionic TbPc₂ molecule. This is expected because the ground quasi-doublet is not a Kramers system.⁴⁴ For the neutral TbPc₂ molecule, the \mathbf{g} matrix has only one large eigenvalue with very small two other eigenvalues ($\sim 10^{-6}$), which can be explained by the fact that the ground doublet is well separated from excited

Table 1: Calculated Elements^a of the Magnetic Hyperfine Matrix in Units of MHz

Molecule	A_{xx}	A_{yy}	A_{zz}	A_{xy}	A_{xz}	A_{yz}	$ A_0 $	$ A_1 $	$ A_2 $
Neutral	0.0	0.0	6145.8	0.0	0.8	0.0	0.0	0.4	0.0
Anionic	0.0	0.0	5992.6	0.0	0.1	-0.5	0.0	0.3	0.0

^a Used the magnetic coordinate system (Fig. 1) in which the \mathbf{g} matrix for the electronic ground doublet is diagonal.

doublets. We choose the z axis to point along the eigenvector corresponding to the large eigenvalue. This direction points approximately perpendicular to the ligand planes. For the anionic TbPc_2 , we find $g_{zz} = 17.993$. This value agrees well with $2g_L J = 18$ (where $g_L = 3/2$ is the Lande g factor for the $S = 3, L = 3, J = 6$ multiplet) as expected for the $M_J = \pm J$ doublet. For the neutral TbPc_2 , we obtain $g_z = 20.003$ which is larger by about two units than the value for the anionic molecule. This difference can be explained by the electronic g factor of the ligand electron. Note that since $g_{xx} = g_{yy} = 0$, the x and y directions are not well defined. Therefore, it is more convenient to use the complex parameters introduced in Eqs. (7) and (14).

Magnetic hyperfine interaction

Table 1 shows the calculated elements of the magnetic hyperfine matrix. For both the neutral and anionic molecules, the A_{zz} element is dominant with the other elements being close to zero. This is expected for large uniaxial magnetic anisotropy. For the entire $J = 6$ ground-multiplet the \mathbf{A} matrix is isotropic as long as interactions with higher multiplets can be neglected.²⁹ Projection on the ground doublet (with a pseudo-spin $S = 1/2$) would then result in the interaction of the form $A_{zz}I_zS_z$. This is, indeed, the case as long as we use coordinate system in which the \mathbf{A} matrix is diagonal. The presence of nonzero A_{xz} and/or A_{yz} elements is due to a slight misalignment between the z axes of the \mathbf{g} matrix and \mathbf{A} matrix coordinate systems. However, A_{xx} , A_{xy} , and A_{yy} terms still remain zero because $g_{xx} = g_{yy} = 0$. For the anionic molecule, this misalignment is caused by the interaction of the $J = 6$ ground-multiplet with higher multiplets.²⁹ In the case of the neutral molecule,

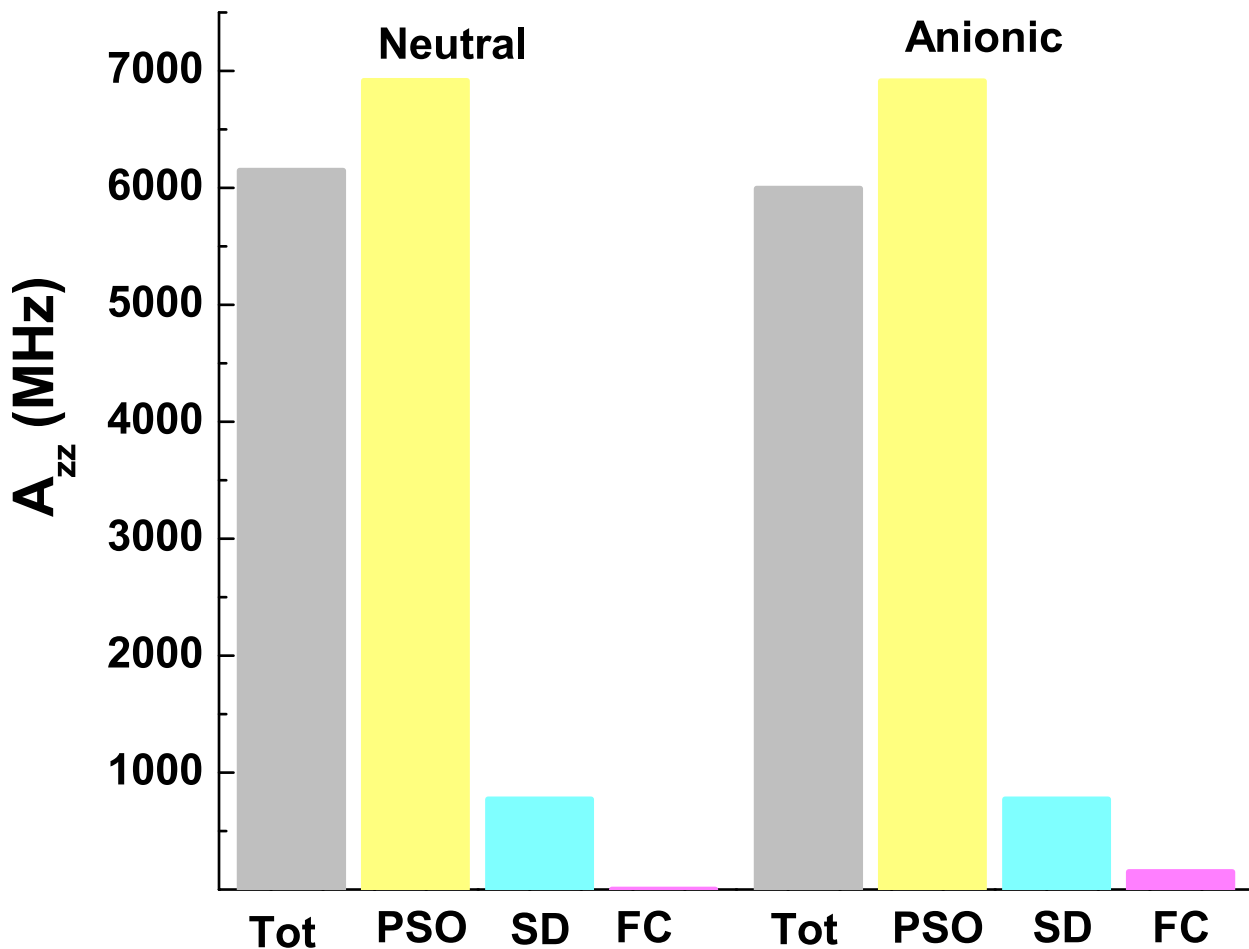


Figure 3: Total (Tot), paramagnetic spin-orbital (PSO), spin-dipole (SD), and Fermi contact (FC) contributions to the calculated A_{zz} element for the neutral and anionic TbPc₂ molecules. For the neutral molecule, the FC contribution is less than 0.1 MHz.

the interaction between the unpaired ligand spin and the ground-multiplet also contributes to this misalignment. Note that the sign of the A_{zz} is undetermined in our calculations.

Overall, the calculated A_{zz} value is about 6000 MHz. In order to understand the origin of such strong hyperfine coupling, we compare PSO, SD and FC contributions to A_{zz} against its total value. See Figure 3. For both molecules, the PSO contribution is dominant due to the presence of the large Tb orbital angular momentum. Both the SD and FC terms have opposite contributions to the PSO term. The SD contribution is much smaller than the PSO part but still significant. The PSO and SD contributions are similar for the neutral and anionic molecules. However, the FC term differs strongly between different TbPc₂

Table 2: Calculated Elements^a of the Nuclear Quadrupole Tensor in Units of MHz for Neutral and Anionic TbPc₂ Molecules

Molecule	P_{xx}	P_{yy}	P_{zz}	P_{xy}	P_{xz}	P_{yz}	$ P_1 $	$ P_2 $
Neutral	-139.1	-147.3	286.4	-0.1	4.7	-0.1	4.7	4.1
Anionic	-54.8	-217.2	272.0	-28.4	9.2	-16.0	18.5	86.0

^a Used the magnetic coordinate system (Fig. 1) in which the \mathbf{g} matrix for the electronic ground doublet is diagonal.

molecules. For the neutral molecule, the FC contribution is negligibly small (< 0.1 MHz). On the other hand, for the anionic molecule, the FC contribution is ≈ 150 MHz. The fact that the FC is smaller than the PSO and SD contributions is not surprising, since the spin density is carried by $4f$ -like orbitals which have zero spin density at the Tb nucleus position. The FC contribution requires hybridization between $4f$ -like and s -like orbitals. Such hybridization would be stronger for the less symmetric anionic molecule, which likely explains a significantly larger FC term for this system. Note that the core-polarization effects are not included in our calculations, and therefore, the FC is expected to be somewhat underestimated. Nevertheless, for Tb³⁺ ion, this effect is expected to be much smaller than the PSO and SD terms.²⁹

Nuclear quadrupole interaction

Table 2 shows the calculated elements of the traceless nuclear quadrupole tensor. We obtain a strong quadrupole interaction with P_{zz} approaching 300 MHz. This is a result of orbital angular momentum carrying asymmetric $4f$ charge distribution which creates a large electric-field gradient at the Tb nucleus. Indeed, we check that the replacement of the Tb ion by a Gd³⁺ ion ($L = 0$) results in a much smaller electric-field gradient. The diagonal P_{zz} parameter is similar for the neutral and anionic TbPc₂. However, the off-diagonal elements (P_1 and P_2) differ significantly between the two TbPc₂ molecules due to different degrees of the structural deviations from the D_{4d} symmetry. For the neutral TbPc₂, the magnitudes of P_1 and P_2 are less than 5 MHz. On the other hand, for the anionic TbPc₂, these parameters

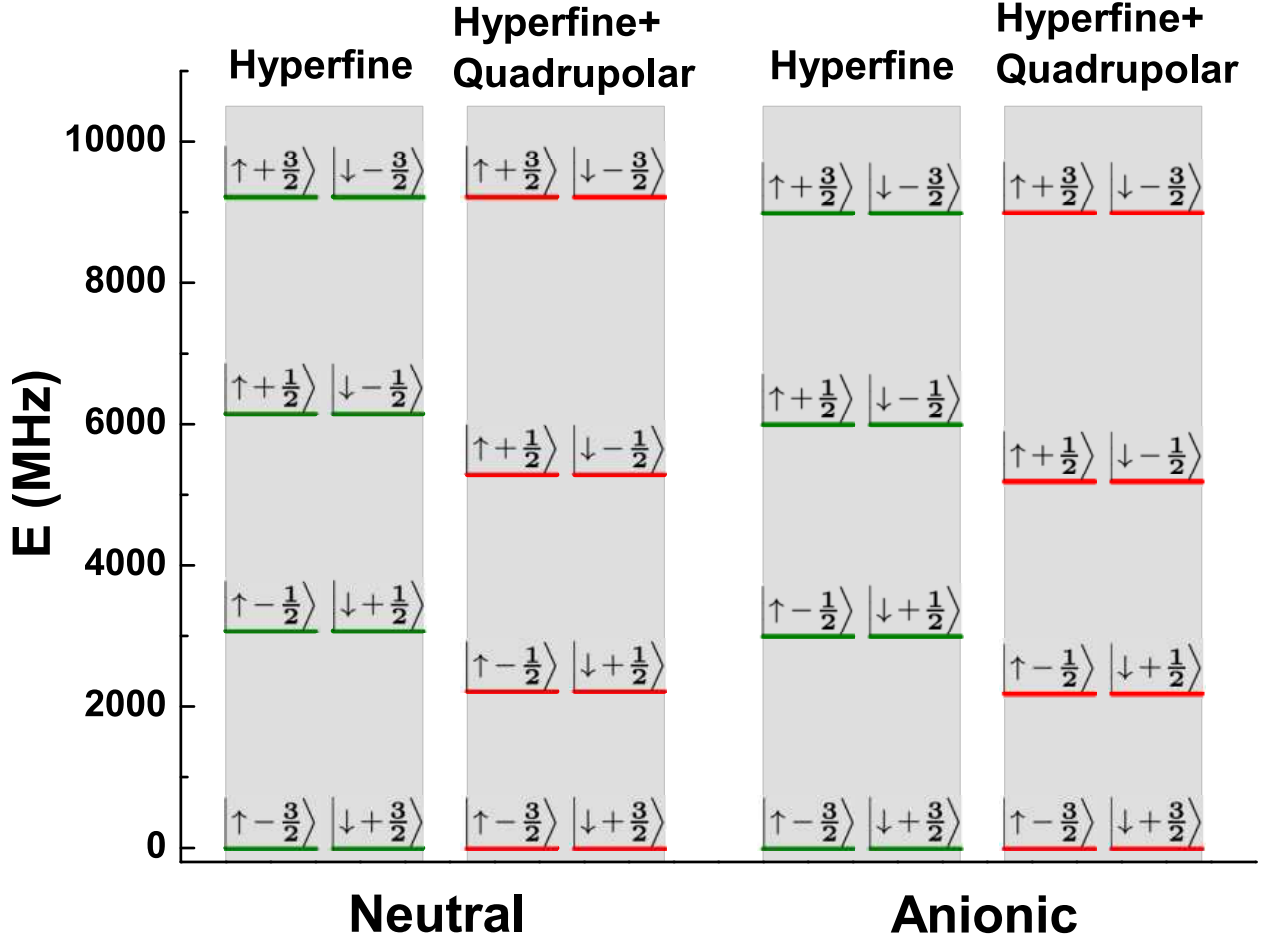


Figure 4: The calculated low-energy electronic-nuclear spectra of the neutral and anionic TbPc_2 molecules. The equally spaced green lines correspond to energy levels found by diagonalization of the magnetic hyperfine Hamiltonian, Eq. (6). The red lines correspond to energy levels found by diagonalization of the sum of the magnetic hyperfine and nuclear quadrupole Hamiltonians [Eqs. (6) and (12)]. The approximate quantum numbers $|M_S, M_I\rangle$ of the calculated energy levels are shown.

are significantly larger with $|P_2|$ being almost third of the P_{zz} value.

Electronic-nuclear energy spectrum

Having calculated the elements of the \mathbf{A} matrix and \mathbf{P} tensor for the electronic ground doublet, we now calculate the low-energy electronic-nuclear spectrum of TbPc_2 . Figure 4 shows the energy levels calculated by diagonalizing the effective pseudo-spin Hamiltonian for the magnetic hyperfine interaction [Eq. (6)] with and without the nuclear quadrupole

Table 3: Calculated and Experimental^a Electronic-Nuclear Relative Energy Levels in GHz

Levels ^b	Neutral	Anionic	Experiment
$E_2 - E_1$	2.214	2.182	2.(5)
$E_3 - E_2$	3.073	3.003	3.(1)
$E_4 - E_3$	3.932	3.812	3.(7)

^a Ref. 8. ^b E_i denotes i^{th} lowest electronic-nuclear doublet.

interaction [Eq. (12)]. For both the neutral and anionic TbPc₂, the spectrum is composed of four doublets. This degeneracy is a consequence of the fact that the \mathbf{A} matrix has only one nonzero eigenvalue. Therefore, at zero magnetic field, the Hamiltonian matrix is block-diagonal with two blocks, one for each S_z value. Within each block, the Hamiltonian matrix describes a $I = 3/2$ system which must be at least doubly degenerate by virtue of the Kramers theorem.

Without the nuclear quadrupole term, the doublets are equidistant with level spacing ~ 3000 MHz. In this case, the pseudo-spin ($M_S = \uparrow, \downarrow$) and nuclear ($M_I = \pm 3/2, \pm 1/2$) magnetic quantum numbers represent the electronic-nuclear states (Fig. 4) since all elements of the \mathbf{A} matrix except A_{zz} are negligible. For the lowest electronic-nuclear doublet the electronic pseudo-spin is antiparallel to the nuclear spin due to our choice of a positive A_{zz} element. Addition of the quadrupole interaction makes the energy levels non-equidistant in agreement with experiment.^{8,15,28} Table 3 compares the experimental relative energy levels⁸ with our calculated values for the neutral and anionic TbPc₂ molecules. Note that this approach is favorable over direct comparison between the theoretical and experimental interaction parameters. In the fitting to the experimental data, a less general Hamiltonian with only two parameters was used.^{8,15,28} The calculated energy levels are similar for the neutral and anionic molecules. In both cases, the calculated values agree well with experiment. This indicates that our methodology is capable of an accurate quantitative description of the electronic-nuclear spectrum of Tb-based SMMs.

The spectrum of the anionic and the neutral molecules are similar even though the two molecules have significantly different off-diagonal \mathbf{P} tensor elements. This indicates that the

transverse quadrupole parameters do not have a large effect on the energy levels. These parameters, however, mix states with different M_I . As a result, the electronic-nuclear states are not pure $|M_S, M_I\rangle$ states and the notation in Fig. 4 is only approximate. The mixing is illustrated in the Supporting Information (Tables S4 and S5) where the eigenvectors of the effective pseudo-spin Hamiltonian are shown for the neutral and anionic TbPc_2 , respectively. The mixing is significantly stronger for the asymmetric anionic molecule with larger off-diagonal \mathbf{P} -tensor elements. The mixing plays an important role in magnetization dynamics (see below).

Zeeman diagram

In order to investigate the role of hyperfine and quadrupole interactions on magnetization dynamics we calculate Zeeman diagram that shows the evolution of electronic-nuclear energy levels as a function of external magnetic field along the z axis (B_z) for the anionic TbPc_2 molecule. The magnetic field is included by considering the Zeeman pseudo-spin Hamiltonian $\hat{H}_Z = \mu_B B_z g_{zz} \hat{S}_z$. Since the anionic molecule is an even-electron system, the ground quasi-doublet has a small tunnel splitting attributed to the transverse CF. This tunnel splitting is crucial for a description of magnetization dynamics because it mixes states with $M_S = \uparrow, \downarrow$ levels, and allows tunneling between different electronic-nuclear levels. For the pseudo-spin $S = 1/2$, the transverse CF can be described by $\hat{H}_{\text{TS}} = \Delta_{\text{TS}} \hat{S}_x$,^{29,44} where Δ_{TS} is the tunnel splitting i.e., the energy splitting between the lowest electronic quasi-doublet. The value of Δ_{TS} depends crucially on the details of TbPc_2 structure.²⁶ In particular, for the asymmetric anionic TbPc_2 of interest, Δ_{TS} is as large as ~ 140 MHz. The full effective pseudo-spin Hamiltonian is, thus,

$$\hat{H}_{\text{eff}} = \hat{H}_A + \hat{H}_Q + \hat{H}_Z + \hat{H}_{\text{TS}}. \quad (17)$$

Figure 5 shows the Zeeman diagram obtained using the parameters calculated for the anionic TbPc_2 molecule. The diagram is symmetric with respect to $B_z \rightarrow -B_z$. The external

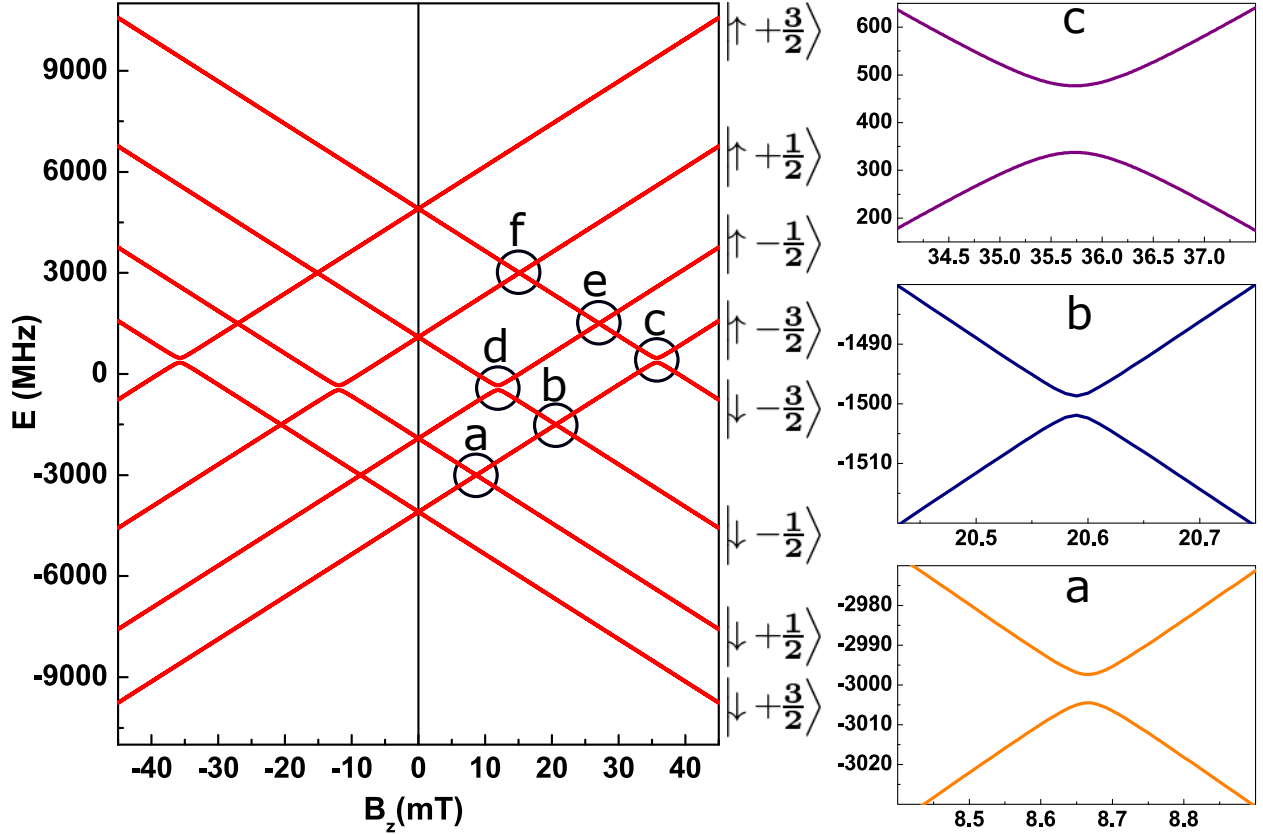


Figure 5: (Left) Zeeman diagram showing the calculated electronic-nuclear energy levels as a function of magnetic field along the z axis (B_z) for the anionic TbPc_2 molecule. Here $|M_S, M_I\rangle$ represents the approximate quantum numbers of the levels away from avoided level crossing points. Black circles denote avoided level crossing points for the positive magnetic fields. (Right) Zoom-ins of three avoided level crossings (a, b and c).

Table 4: Characteristics of Avoided Level Crossings for Positive Magnetic Fields for the Anionic TbPc_2 Molecule

	B_{ALC} (mT)	ΔE_{ALC} (MHz)	$ \Delta M_{\text{ALC}} $
a	8.67	7	2
b	20.59	3	1
c	35.73	140	0
d	11.93	140	0
e	27.07	3	1
f	15.14	7	2

magnetic field breaks the zero-field two-fold degeneracy. At certain magnetic field values, the levels with opposite M_S cross. For positive fields, these crossing points are denoted by black circles in Fig. 5. Zooming the area around the crossing points reveals that the levels

do not actually cross and there is a finite gap between them (see zoom-ins on the right of Fig. 5). We have, thus, avoided level crossings (ALCs). At positive fields, there are six such ALCs. The magnetic field value B_{ALC} and the width of the gap ΔE_{ALC} for each of these ALCs are shown in Table 4. In addition, Table 4 provides the magnitude of the difference between M_I of the two crossing levels $|\Delta M_{\text{AC}}|$. There are two ALCs with $|\Delta M_{\text{AC}}| = 0$, two with $|\Delta M_{\text{ALC}}| = 1$, and two with $|\Delta M_{\text{ALC}}| = 2$. ALCs with the same $|\Delta M_{\text{ALC}}|$ have equal values of ΔE_{ALC} . ALCs with $|\Delta M_{\text{ALC}}| = 0$ have a significant gap that is roughly equal to Δ_{TS} . Indeed, in this case the wave functions of the crossing levels can be approximated by pure $|M_S, M_I\rangle$ states and $\Delta E_{\text{ALC}} \approx 2|\langle \uparrow M_I | \hat{H}_{\text{eff}} | \downarrow M_I \rangle| = \Delta_{\text{TS}}$. However, for $|\Delta M_{\text{ALC}}| \neq 0$, $\langle \uparrow M_I | \hat{H}_{\text{eff}} | \downarrow M_I' \rangle = 0$ and, therefore, we need to take into account the mixing between the states with different M_I . Using perturbation theory, it can be shown that for $|\Delta M_{\text{ALC}}| = 1$, the ALC gap is controlled by terms like $\frac{\Delta_{\text{TS}}|P_1|}{E_2 - E_1}$ and $\frac{\Delta_{\text{TS}}|P_1|}{E_3 - E_2}$. Similarly, for $|\Delta M_{\text{ALC}}| = 2$, terms like $\frac{\Delta_{\text{TS}}|P_2|}{E_3 - E_1}$ and $\frac{\Delta_{\text{TS}}|P_2|}{E_4 - E_2}$ determine the ALC gap. Note that in this case the denominators are significantly larger but since, for the anionic TbPc₂, $|P_2| > |P_1|$, the corresponding ΔE_{ALC} is still larger than for $|\Delta M_{\text{ALC}}| = 1$.

ALCs are essential for low-temperature magnetization dynamics of TbPc₂ SMMs. The ALC gap determines the tunneling probability between different electronic-nuclear levels as the magnetic field is swept with a fixed rate $|dB_z/dt|$. The probability is given by the Landau-Zener formula⁴⁵

$$P_{\text{LZ}} = 1 - \exp\left(-\frac{\pi \Delta E_{\text{ALC}}^2}{2\hbar \mu_B g_{zz} |dB_z/dt|}\right) \quad (18)$$

Clearly, the tunneling probability is the largest for ALCs with the largest ΔE_{ALC} that is ALCs with $|\Delta M_{\text{ALC}}| = 0$. The tunneling transitions with $|\Delta M_{\text{AC}}| \neq 0$ can also occur as long as significant transverse quadrupole interaction parameters are present. Such transitions have recently been observed.⁴⁶

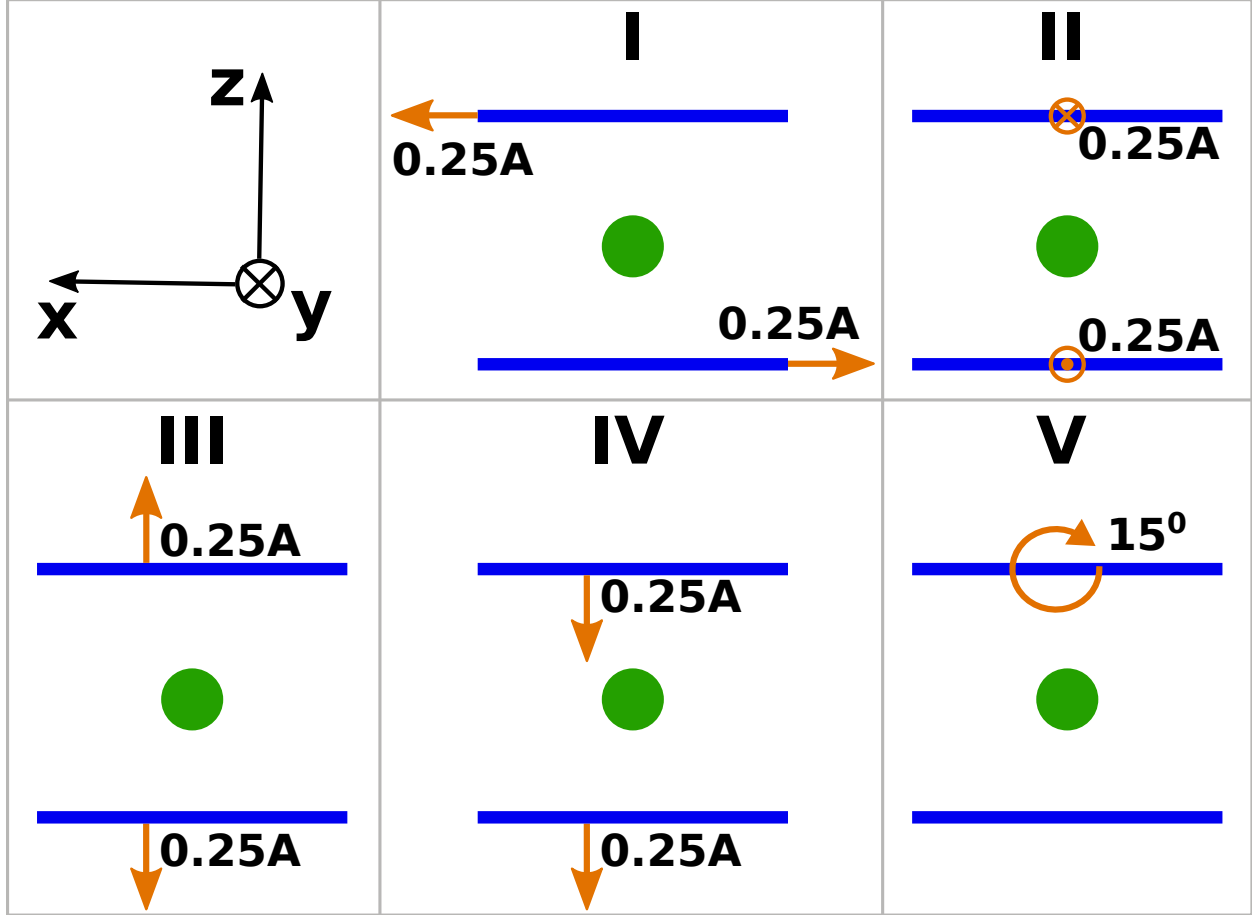


Figure 6: Schematic illustration of five types of molecular distortions (denoted by roman letters) applied to the anionic TbPc_2 . See the main text for the description of the distortions.

Effect of geometry distortion

In previous sections, we demonstrate that the transverse quadrupole parameters for the TbPc_2 molecule can vary significantly depending on differences in molecular structures. In order to investigate the effect of molecular distortion on hyperfine interactions in a more systematic manner we apply five types of ligand distortions to the anionic TbPc_2 , as shown in Fig. 6: (I) Two Pc ligands displaced along the x axis in the opposite direction to each other by 0.25 \AA , (II) Pc ligands displaced along the y axis in the opposite direction to each other by 0.25 \AA , (III) Pc ligands displaced along the z axis in the opposite direction to each other by 0.25 \AA , (IV) Pc ligands displaced along the z axis in the same direction by 0.25 \AA , and (V) one of the Pc ligands rotated in the xy plane by 15° .

Table 5: Calculated Hyperfine and Quadrupole Parameters, Relative Electronic-Nuclear Energy Levels, and Tunnel Splitting for Different Distorted Geometries^a of the Anionic TbPc₂ Molecule in Units of MHz

	A_{zz}	$ A_0 $	$ A_1 $	$ A_2 $	P_{zz}	$ P_1 $	$ P_2 $	$E_2 - E_1$	$E_3 - E_2$	$E_4 - E_3$	Δ_{TS}
I	5951.0	0.0	0.6	0.0	240.3	127.8	82.5	2298	2948	3722	90
II	5950.0	0.0	0.9	0.0	208.6	125.2	66.5	2389	2946	3626	90
III	5873.1	0.0	0.3	0.0	311.0	21.8	104.7	2520	3460	4383	870
IV	6082.7	0.0	0.1	0.0	203.7	8.4	60.0	2853	3467	4075	30
V	6038.4	0.0	0.4	0.0	264.4	20.6	122.8	2229	3034	3811	180

^a See Fig. 6.

Table 5 shows the hyperfine and quadrupole parameters, electronic-nuclear energy levels as well as tunnel splittings calculated for the five types of distortions of the anionic TbPc₂ molecule. We find that the PSO and SD contributions to A_{zz} are insensitive to molecular distortions. On the other hand, the FC term shows significant variation under considered distortions which is primarily responsible for the changes of A_{zz} in Table 5. In particular, the FC term increases for types I, II and III resulting in a decrease of the total A_{zz} since FC term is opposite to the dominant PSO contribution. For types IV and V, the FC term is reduced and the total A_{zz} value is enhanced. This result indicates that a potential route for an external control of the magnetic hyperfine interactions of the Tb nucleus in the Tb-based SMMs should involve modification of the FC contribution.

The diagonal quadrupole parameter P_{zz} shows considerable variation under geometry distortions. This parameter is responsible for non-equidistant electronic nuclear spectrum which is crucial for an efficient readout of nuclear spin.^{8,15} For type III, the ligands are pulled away from the Tb ion reducing the hybridization between the $4f$ -like states and ligand orbitals. This increases the electric-field gradient at the Tb nucleus position and enhances P_{zz} . On the other hand, for types I, II and IV, the distortion increases hybridization of the Tb-ligand hybridization and reduces P_{zz} . Type V does not significantly affect the hybridization and, therefore, only a small change of P_{zz} is found.

Transverse quadrupole parameters are strongly affected by geometry distortions. In particular, for types I and II, $|P_1|$ increases by an order of magnitude. As a result, the gap

of $|\Delta M_{\text{ALC}}| = 1$ ALCs is significantly enhanced (Table S6 in the Supporting Information). This enhancement is, however, reduced by a decrease of Δ_{TS} under type I and II distortions (Table 5). In fact, using Δ_{TS} for the undistorted anionic TbPc_2 structure, we obtain even larger $|\Delta M_{\text{ALC}}| = 1$ ALC gap for types I and II distortions (Table S7 in Supporting Information). Therefore, magnetization tunneling processes can significantly increase for certain structural distortions.

Conclusions

We investigate magnetic hyperfine and nuclear quadrupole interactions for ^{159}Tb nucleus in TbPc_2 SMMs using multireference *ab initio* calculations including SOI and the effective pseudo-spin Hamiltonian method. The key findings are as follows:

- The strong uniaxial magnetic hyperfine interaction ($A_{zz} \sim 6000$ MHz) is dominated by the PSO mechanism.
- Different experimental geometries have similar PSO and SD contributions to the magnetic hyperfine interaction, whereas the FC term shows a strong dependence on details of molecular geometry and becomes significant for less symmetric molecules.
- Asymmetric $4f$ charge distribution leads to a large diagonal quadrupole interaction ($P_{zz} \sim 300$ MHz). For less symmetric molecular geometries, the transverse quadrupole parameters become significant.
- The electronic-nuclear spectrum obtained by diagonalization of the effective pseudo-spin Hamiltonian is in excellent agreement with experiment.
- The analysis of the calculated Zeeman diagram for the asymmetric anionic TbPc_2 molecule reveals that transverse quadrupole parameters allow for magnetization tunneling processes that do not conserve nuclear spin.

- We demonstrate that small distortions of molecular geometry can affect hyperfine parameters with strong sensitivity of transverse quadrupole parameters to details of the molecular structure.

Acknowledgement

This work was funded by the Department of Energy (DOE) Basic Energy Sciences (BES) grant No de-sc0018326. Computational support by Virginia Tech ARC and San Diego Supercomputer Center (SDSC) under DMR060009N. The authors are grateful to Dr. Kamal Sharkas for insightful discussion at the earlier stage of this work.

Supporting Information Available

The following files are available free of charge. The Supporting Information is available free of charge: Active space dependence, hyperfine calculations tests, pseudo-spin Hamiltonian eigenvectors, and avoided level crossing gaps for the distorted geometries.

References

- (1) Strategies Towards Single Molecule Magnets Based on Lanthanide Ions. *Coord. Chem. Rev.* **2009**, *253*, 2328 – 2341.
- (2) Baldoví, J. J.; Cardona-Serra, S.; Clemente-Juan, J. M.; Coronado, E.; Gaita-Ariño, A.; Pali, A. Rational Design of Single-Ion Magnets and Spin Qubits Based on Mononuclear Lanthanoid Complexes. *Inorg. Chem.* **2012**, *51*, 12565–12574.
- (3) Woodruff, D. N.; Winpenny, R. E. P.; Layfield, R. A. Lanthanide Single-Molecule Magnets. *Chem. Rev.* **2013**, *113*, 5110–5148.

- (4) Liddle, S. T.; van Slageren, J. Improving f-Element Single Molecule Magnets. *Chem. Soc. Rev.* **2015**, *44*, 6655–6669.
- (5) Single-Molecule Magnetism of Tetrapyrrole Lanthanide Compounds with Sandwich Multiple-Decker Structures. *Coord. Chem. Rev.* **2016**, *306*, 195 – 216.
- (6) Guo, F.-S.; Day, B. M.; Chen, Y.-C.; Tong, M.-L.; Mansikkamäki, A.; Layfield, R. A. Magnetic Hysteresis up to 80 Kelvin in a Dysprosium Metallocene Single-Molecule Magnet. *Science* **2018**, *362*, 1400–1403.
- (7) Goodwin, C.; Ortu, F.; Reta, D.; Chilton, N.; Mills, D. Molecular Magnetic Hysteresis at 60 Kelvin in Dysprosocenium. *Nature* **2017**, *548*, 439–442.
- (8) Thiele, S.; Balestro, F.; Ballou, R.; Klyatskaya, S.; Ruben, M.; Wernsdorfer, W. Electrically Driven Nuclear Spin Resonance in Single-Molecule Magnets. *Science* **2014**, *344*, 1135–1138.
- (9) Godfrin, C.; Ferhat, A.; Ballou, R.; Klyatskaya, S.; Ruben, M.; Wernsdorfer, W.; Balestro, F. Operating Quantum States in Single Magnetic Molecules: Implementation of Grover’s Quantum Algorithm. *Phys. Rev. Lett.* **2017**, *119*, 187702.
- (10) Ishikawa, N.; Sugita, M.; Ishikawa, T.; Koshihara, S.-y.; Kaizu, Y. Lanthanide Double-Decker Complexes Functioning as Magnets at the Single-Molecular Level. *J. Am. Chem. Soc.* **2003**, *125*, 8694–8695.
- (11) He, Y.; Zhang, Y.; Hong, I.-P.; Cheng, F.; Zhou, X.; Shen, Q.; Li, J.; Wang, Y.; Jiang, J.; Wu, K. Low-Temperature Scanning Tunneling Microscopy Study of Double-Decker DyPc₂ on Pb Surface. *Nanoscale* **2014**, *6*, 10779–10783.
- (12) Wckerlin, C.; Donati, F.; Singha, A.; Baltic, R.; Rusponi, S.; Diller, K.; Patthey, F.; Pivetta, M.; Lan, Y.; Klyatskaya, S.; Ruben, M.; Brune, H.; Dreiser, J. Giant Hysteresis

- of Single-Molecule Magnets Adsorbed on a Nonmagnetic Insulator. *Adv. Mater.* **28**, 5195–5199.
- (13) Studniarek, M.; Wckerlin, C.; Singha, A.; Baltic, R.; Diller, K.; Donati, F.; Rusponi, S.; Brune, H.; Lan, Y.; Klyatskaya, S.; Ruben, M.; Seitsonen, A. P.; Dreiser, J. Understanding the Superior Stability of Single-Molecule Magnets on an Oxide Film. *Adv. Sci.* **0**, 1901736.
- (14) Ishikawa, N.; Sugita, M.; Ishikawa, T.; Koshihara, S.-y.; Kaizu, Y. Mononuclear Lanthanide Complexes with a Long Magnetization Relaxation Time at High Temperatures: A New Category of Magnets at the Single-Molecular Level. *J. Phys. Chem. B* **2004**, *108*, 11265–11271.
- (15) Vincent, R.; Klyatskaya, S. V.; Ruben, M.; Wernsdorfer, W.; Balestro, F. Electronic Read-out of a Single Nuclear Spin Using a Molecular Spin Transistor. *Nature* **2012**, *488*, 357–360.
- (16) Urdampilleta, M.; Klyatskaya, S.; Ruben, M.; Wernsdorfer, W. Landau-Zener Tunneling of a Single Tb^{3+} Magnetic Moment Allowing the Electronic Read-out of a Nuclear Spin. *Phys. Rev. B* **2013**, *87*, 195412.
- (17) Thiele, S.; Vincent, R.; Holzmann, M.; Klyatskaya, S.; Ruben, M.; Balestro, F.; Wernsdorfer, W. Electrical Readout of Individual Nuclear Spin Trajectories in a Single-Molecule Magnet Spin Transistor. *Phys. Rev. Lett.* **2013**, *111*, 037203.
- (18) Godfrin, C.; Ballou, R.; Bonet, E.; Ruben, M.; Klyatskaya, S.; Wernsdorfer, W.; Balestro, F. Generalized Ramsey Interferometry Explored with a Single Nuclear Spin Qudit. *npj Quantum Inf.* **2018**, *4*.
- (19) Komijani, D.; Ghirri, A.; Bonizzoni, C.; Klyatskaya, S.; Moreno-Pineda, E.; Ruben, M.; Soncini, A.; Affronte, M.; Hill, S. Radical-Lanthanide Ferromagnetic Interaction in a Tb^{III} Bis-phthalocyaninato Complex. *Phys. Rev. Materials* **2018**, *2*, 024405.

- (20) Branzoli, F.; Carretta, P.; Filibian, M.; Zoppellaro, G.; Graf, M. J.; Galan-Mascaros, J. R.; Fuhr, O.; Brink, S.; Ruben, M. Spin Dynamics in the Negatively Charged Terbium (III) Bis-phthalocyaninato Complex. *J. Am. Chem. Soc.* **2009**, *131*, 4387–4396.
- (21) Ishikawa, N.; Sugita, M.; Tanaka, N.; Ishikawa, T.; Koshihara, S.; Kaizu, Y. Upward Temperature Shift of the Intrinsic Phase Lag of the Magnetization of Bis(phthalocyaninato)terbium by Ligand Oxidation Creating an $S = 1/2$ Spin. *Inorg. Chem.* **2004**, *43*, 5498–5500.
- (22) Loosli, C.; Liu, S.-X.; Neels, A.; Labat, G.; Decurtins, S. Crystal Structures of Tetrabutylammonium Bis(phthalocyaninato)terbium(III) Methanol Solvate Hydrate $[\text{N}(\text{C}_4\text{H}_9)_4][\text{Tb}(\text{C}_8\text{H}_4\text{N}_2)_2]\text{CH}_3\text{OH}_3/2\text{H}_2\text{O}$, and Tetrabutylammonium Bis(phthalocyaninato)dysprosium(III) Methanol Solvate Hydrate $[\text{N}(\text{C}_4\text{H}_9)_4][\text{Dy}(\text{C}_8\text{H}_4\text{N}_2)_2]\text{CH}_3\text{OHH}_2\text{O}$. *Z. Kristallogr. Cryst. Mater* **2006**, *221*, 135–141.
- (23) Takamatsu, S.; Ishikawa, T.; Koshihara, S.-y.; Ishikawa, N. Significant Increase of the Barrier Energy for Magnetization Reversal of a Single- $4f$ -Ionic Single-Molecule Magnet by a Longitudinal Contraction of the Coordination Space. *Inorg. Chem.* **2007**, *46*, 7250–7252.
- (24) Katoh, K.; Yoshida, Y.; Yamashita, M.; Miyasaka, H.; Breedlove, B. K.; Kajiwara, T.; Takaishi, S.; Ishikawa, N.; Isshiki, H.; Zhang, Y. F.; Komeda, T.; Yamagishi, M.; Takeya, J. Direct Observation of Lanthanide(III)-Phthalocyanine Molecules on Au(111) by Using Scanning Tunneling Microscopy and Scanning Tunneling Spectroscopy and Thin-Film Field-Effect Transistor Properties of Tb(III)- and Dy(III)-Phthalocyanine Molecules. *J. Am. Chem. Soc.* **2009**, *131*, 9967–9976.
- (25) Ganivet, C. R.; Ballesteros, B.; de la Torre, G.; Clemente-Juan, J. M.; Coronado, E.;

- Torres, T. Influence of Peripheral Substitution on the Magnetic Behavior of Single-Ion Magnets Based on Homo- and Heteroleptic TbIII Bis(phthalocyaninate). *Chem. Eur. J* **2013**, *19*, 1457–1465.
- (26) Pederson, R.; Wysocki, A. L.; Mayhall, N.; Park, K. Multireference Ab Initio Studies of Magnetic Properties of Terbium-Based Single-Molecule Magnets. *J. Phys. Chem. A* **2019**, *123*, 6996–7006.
- (27) Ungur, L.; Chibotaru, L. F. Ab Initio Crystal Field for Lanthanides. *Chem. Eur. J* **2017**, *23*, 3708–3718.
- (28) Ishikawa, N.; Sugita, M.; Wernsdorfer, W. Quantum Tunneling of Magnetization in Lanthanide Single-Molecule Magnets: Bis(phthalocyaninato)terbium and Bis(phthalocyaninato)dysprosium Anions. *Angew. Chem.* *44*, 2931–2935.
- (29) Abragam, A.; Bleaney, B. *Electron Paramagnetic Resonance of Transition Ions*; Clarendon Press: Oxford, 1970.
- (30) Bolvin, H.; Autschbach, J. In *Handbook of Relativistic Quantum Chemistry*; Liu, W., Ed.; Springer Berlin Heidelberg: Berlin, Heidelberg, 2014; pp 1–39.
- (31) Sharkas, K.; Pritchard, B.; Autschbach, J. Effects from Spin-Orbit Coupling on Electron-Nucleus Hyperfine Coupling Calculated at the Restricted Active Space Level for Kramers Doublets. *J. Chem. Theory Comput.* **2015**, *11*, 538–549.
- (32) Autschbach, J.; Zheng, S.; Schurko, R. W. Analysis of Electric Field Gradient Tensors at Quadrupolar Nuclei in Common Structural Motifs. *Concepts Magn. Reson. Part A* *36A*, 84–126.
- (33) Pyykk, P. Year-2008 Nuclear Quadrupole Moments. *Mol. Phys.* **2008**, *106*, 1965–1974.
- (34) Aquilante, F. et al. Molcas 8: New Capabilities for Multiconfigurational Quantum

- Chemical Calculations across the Periodic Table. *J. Comput. Chem.* **2016**, *37*, 506–541.
- (35) Douglas, M.; Kroll, N. M. Quantum Electrodynamical Corrections to the Fine Structure of Helium. *Ann. Phys.* **1974**, *82*, 89–155.
- (36) Hess, B. A. Relativistic Electronic-Structure Calculations Employing a Two-Component No-Pair Formalism with External-Field Projection Operators. *Phys. Rev. A* **1986**, *33*, 3742–3748.
- (37) Widmark, P.-O.; Malmqvist, P.-Å.; Roos, B. O. Density Matrix Averaged Atomic Natural Orbital (ANO) Basis Sets for Correlated Molecular Wave Functions. *Theor. Chem. Acc.* **1990**, *77*, 291–306.
- (38) Roos, B. O.; Lindh, R.; Malmqvist, P.-Å.; Veryazov, V.; Widmark, P.-O. Main Group Atoms and Dimers Studied with a New Relativistic ANO Basis Set. *J. Phys. Chem. A* **2004**, *108*, 2851–2858.
- (39) Roos, B. O.; Taylor, P. R.; Siegbahn, P. E. M. A Complete Active Space SCF Method (CASSCF) Using a Density Matrix Formulated Super-CI Approach. *Chem. Phys.* **1980**, *48*, 157–173.
- (40) Siegbahn, P. E. M.; Almlöf, J.; Heiberg, A.; Roos, B. O. The Complete Active Space SCF (CASSCF) Method in a Newton-Raphson Formulation with Application to the HNO Molecule. *J. Chem. Phys.* **1981**, *74*, 2384–2396.
- (41) Hess, B. A.; Marian, C. M.; Wahlgren, U.; Gropen, O. A Mean-Field Spin-Orbit Method Applicable to Correlated Wavefunctions. *Chem. Phys. Lett.* **1996**, *251*, 365 – 371.
- (42) Malmqvist, P.-Å.; Roos, B. O.; Schimmelpfennig, B. The Restricted Active Space (RAS) State Interaction Approach with Spin-Orbit Coupling. *Chem. Phys. Lett.* **2002**, *357*, 230–240.

- (43) Lan, T. N.; Kurashige, Y.; Yanai, T. Toward Reliable Prediction of Hyperfine Coupling Constants Using Ab Initio Density Matrix Renormalization Group Method: Diatomic 2 and Vinyl Radicals as Test Cases. *J. Chem. Theory Comput.* **2014**, *10*, 1953–1967.
- (44) Griffith, J. S. Spin Hamiltonian for Even-Electron Systems Having Even Multiplicity. *Phys. Rev.* **1963**, *132*, 316–319.
- (45) Wernsdorfer, W.; Sessoli, R.; Caneschi, A.; Gatteschi, D.; Cornia, A.; Maily, D. Landau-Zener Method to Study Quantum Phase Interference of Fe₈ Molecular Nanomagnets (Invited). *J. Appl. Phys.* **2000**, *87*, 5481–5486.
- (46) Taran, G.; Bonet, E.; Wernsdorfer, W. The Role of the Quadrupolar Interaction in the Tunneling Dynamics of Lanthanide Molecular Magnets. *J. Appl. Phys.* **2019**, *125*, 142903.

Synopsis

Hyperfine interactions for ^{159}Tb nucleus in TbPc_2 single-molecule magnets are investigated from first principles using multireference calculations. Strong nuclear quadrupole and magnetic hyperfine coupling are found with the latter being dominated by the paramagnetic spin-orbital mechanism. We construct an *ab initio* pseudo-spin Hamiltonian and obtain the electronic-nuclear spectrum that is in excellent agreement with experiment. The Zeeman diagram is calculated and the magnetization dynamics is discussed. The effects of molecular distortions are studied.

TOC Graphic

